Acta Materialia 101 (2015) 101–106

Contents lists available at ScienceDirect

Acta Materialia

journal homepage: www.elsevier.com/locate/actamat

Strain measurements from $Nd_2Fe_{14}B$ grains in sintered magnets using artificial moiré fringes

Y. Murakami [a,b,d,*], T.T. Sasaki [c,d], T. Ohkubo [c,d], K. Hono [c,d]

[a] Department of Applied Quantum Physics and Nuclear Engineering, Kyushu University, Fukuoka 819-0395, Japan
[b] The Ultramicroscopy Research Center, Kyushu University, Fukuoka 819-0395, Japan
[c] Elements Strategy Initiative Center for Magnetic Materials (ESICMM), National Institute for Materials Science, Tsukuba 305-0047, Japan
[d] JST, CREST, Tsukuba 305-0047, Japan

ARTICLE INFO

Article history:
Received 23 July 2015
Revised 25 August 2015
Accepted 25 August 2015

Keywords:
Permanent magnets
Coercivity
Nanostructure
Grain boundary
Transmission electron microscopy

ABSTRACT

Strain maps for $Nd_2Fe_{14}B$ grains in Nd–Fe–B sintered magnets, representing elongation/contraction in the spacing of *c* planes, have been revealed by analyzing artificial moiré fringes in scanning transmission electron microscopy images. The strain maps were collected from several types of $Nd_2Fe_{14}B$ grains in contact with metallic-Nd (m-Nd), Nd_2O_3, NdO_x, and thin grain boundary phases. A maximum value of strain of ~1.2% was observed at a $Nd_2Fe_{14}B$/m-Nd interface. The magnitude of strain for the interfaces with Nd_2O_3 and NdO_x phases was 0.4–0.5%. The strain was negligible in the vicinity of the grain boundary phase. It appears that the observations are smaller than the theoretical values of strain that may cause a significant change in the magnetocrystalline anisotropy of the $Nd_2Fe_{14}B$ phase.

1. Introduction

The Nd–Fe–B sintered magnet has attracted considerable attention over the last three decades as a permanent magnet with the highest maximum energy product (>400 kJ/m^3) [1–3]. The large energy product enables significant miniaturization of motors and actuators, thereby improving the energy efficiencies of various electrical appliances, industrial machines and electric vehicles that utilize motors and generators. The coercivity of the standard Nd–Fe–B magnets at room temperature is ~1.2 T, which is too low for certain applications such as traction motors of electric vehicles and wind turbines. This value is only ~20% of the theoretical upper limit of coercivity for coherent rotation, *i.e.*, $\mu_0 H_A$ ~7 T, where μ_0 and H_A stand for the permeability in vacuum and the anisotropy field of the $Nd_2Fe_{14}B$ matrix phase, respectively. The other problem is that the coercivity is reduced significantly at elevated temperatures. For example, the coercivity of Nd–Fe–B magnets is only ~0.2 T at 470 K that is the operation temperature of the motors used in hybrid electric vehicles. High temperature applications accordingly require partial substitution of Dy for Nd, *i.e.*, the substitution of Dy for approximately 30% of Nd for increasing the anisotropy field in the $Nd_2Fe_{14}B$ main phase [2,4,5].

Detailed studies of the microstructures of Nd–Fe–B sintered magnets are crucial for a deeper understanding of the coercivity mechanism. The critical microstructural feature that influences the coercivity is considered to be the ultrathin grain boundary phase which envelopes individual $Nd_2Fe_{14}B$ grains [7,9]. Although the grain boundary phase had been believed to be a nonmagnetic phase [6–12], which is favorable for avoiding avalanche-propagation of magnetization reversal, recent three-dimensional atom probe study by Sepehri-Amin et al. [13] reported an unexpectedly high concentration of Fe (~63%) within the thin grain boundary phase. Interestingly, ferromagnetism was observed in a sputtered, thin-film model specimen with the chemical composition close to that determined by the atom probe study. The ferromagnetism of the grain boundary phase was later confirmed by direct magnetization measurements from actual specimens of Nd–Fe–B sintered magnets using electron holography [14], spin-polarized scanning electron microscopy [15], and X-ray magnetic circular dichroism measurements [16].

Another essential problem concerning the microstructure of the sintered magnets is the impact of lattice strain on the magnetocrystalline anisotropy in the $Nd_2Fe_{14}B$ phase. Although the $Nd_2Fe_{14}B$ phase shows a large magnetocrystalline anisotropy constant, $K_u \approx 4.5$ MJ/m^3, theoretical calculations predict that this value could be reduced by orders of magnitude in the presence of significant lattice deformation [17,18]. However, since the complex microstructure hampers intensive diffraction studies, we

* Corresponding author at: Department of Applied Quantum Physics and Nuclear Engineering, Kyushu University, Fukuoka 819-0395, Japan.
E-mail address: murakami@nucl.kyushu-u.ac.jp (Y. Murakami).

http://dx.doi.org/10.1016/j.actamat.2015.08.058
1359-6454/

do not have comprehensive data on lattice strain in the Nd–Fe–B sintered magnets, *i.e.,* direct strain measurements from actual sintered magnets have not been reported so far. In the absence of direct observations, it is difficult to understand the practical role of lattice strain on the coercivity. These points motivated us to carry out strain measurements of Nd–Fe–B sintered magnets using transmission electron microscopy (TEM).

Strain measurements from thin-foil crystals have been carried out using several techniques of TEM, including geometric phase analysis (GPA) method [19,20], convergent beam electron diffraction (CBED) [21,22], nanobeam electron diffraction [23,24], and dark-field electron holography [25,26]. Although each of these methods has advantages and drawbacks, CBED achieves the highest precision of the order of 0.01% *via* the analysis of diffraction lines from higher-order Laue zones (HOLZ). However, the HOLZ lines are obscured in the presence of a strain gradient within the area illuminated by the electron beam, resulting in difficulties in observing specimens with complex microstructures. GPA and nanobeam diffraction are time consuming for collecting strain maps from a wide area of the crystal of the order of 100 nm or larger. A strong magnetic field hampers the precise analysis of lattice displacements using dark-field electron holography, which analyzes the phase shift of incident electrons. In this study, we employed a method that analyzes artificial moiré fringes produced in high-angle annular dark-field scanning transmission electron microscopy (HAADF-STEM) images [27–32] to acquire strain maps from the Nd–Fe–B sintered magnets. As illustrated in Fig. 1, the superposition of the scanning probe, *i.e.,* a type of grating for acquisition of HAADF-STEM images, and the lattice in the crystal produces a low frequency modulation in the image, referred to as artificial moiré fringes (or scanning moiré fringes). Like the conventional moiré fringes generated by two overlapping crystals [33], deviation in the lattice spacing can be recognized as frequency modulation in artificial moiré fringes; this relationship allows sensitive strain measurements using the moiré fringes [27–32]. In addition, this method enables to map strain distribution in the $Nd_2Fe_{14}B$ grains, over a wide area including precipitates and/or other structural imperfections.

In this study, strain maps representing the deformation along the c axis in the $Nd_2Fe_{14}B$ lattice were collected from a commercial sintered magnet. The $Nd_2Fe_{14}B$ grains in contact with several types of precipitates; *i.e.,* the metallic-Nd (m-Nd) phase, the Nd_2O_3 phase, the NdO_x phase, and the ultrathin grain boundary phase. The observations revealed highly strained regions within the sintered magnet subjected to optimal heat treatment, and provided numerical strain data that can be used for theoretical/experimental studies on the magnetoelastic interplay in the Nd–Fe–B sintered magnets.

2. Experimental procedure

The Nd–Fe–B magnet used in this study was a 400 kJ/m^3 grade commercial sintered magnet with a nominal composition of $Nd_{10.9}Pr_{3.1}Fe_{77.4}Co_{2.4}B_{6.0}Ga_{0.1}Cu_{0.1}$ (at%), coercivity of $\mu_0 H_c$ = 1.2 T and remanence of $\mu_0 M_r$ = 1.4 T. Thin-foil specimens for TEM observations were prepared using a focused ion beam (FIB) system (Helios Nanolab 650, FEI) with an acceleration voltage of 30 kV. To reduce surface damage, the foils were polished using a Ga ion beam with a low acceleration voltage (5 kV) at the final stage of specimen preparation. Cross-sectional scanning ion microscopy observations estimated the specimen thickness to be approximately 100 nm.

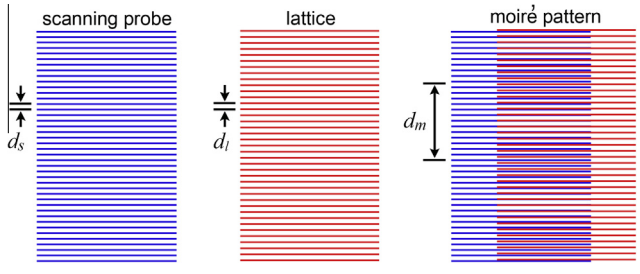

Fig. 1. Schematic representation of the formation of artificial moiré fringes.

HAADF-STEM images, which reveal artificial moiré fringes containing the strain information, were collected from the thin-foil specimens in a scanning transmission electron microscope, TITAN G2 80-200, FEI, with an acceleration voltage of 200 kV. The subsequent section includes details on the formation mechanism of the artificial moiré fringes, and the relationship between the lattice deformation and the moiré fringes. Some of the images were obtained by using another microscope, JEM ARM-200F, JEOL, with an acceleration voltage of 200 kV. The crystal phases in the thin-foil specimens (*i.e.,* $Nd_2Fe_{14}B$, m-Nd, Nd_2O_3, and NdO_x) were identified by electron energy-loss spectroscopy and energy dispersive X-ray spectroscopy. In addition, these phases could be identified by image contrast in scanning electron microscopy (SEM) observations using the in-lens detector equipped in the Helios Nanolab 650, FEI. The emission efficiency of secondary electrons depends on the crystal phases [34].

Here, we describe uncertainty in the strain measurement using artificial moiré fringes. In order to reduce undesired mechanical drift during the image acquisition of 512 × 512 pixel size for each image, the dwell time at each pixel point was fixed at 8 μs. Because of insufficient image intensity due to the short acquisition time, the original moiré patterns and/or phase maps did not allow precise strain measurement. In order to improve the signal-to-noise ratio in the observations from each field of view, 20 raw phase images such as Fig. 3(b) were averaged after careful position fitting between those images. The strain maps determined by this process showed an uncertainty of ±0.2%, which was evaluated from the fluctuations in the strain curves such as those shown in Fig. 3 (d) and (e). Another source of ambiguity is the lattice rotation that may occur in the crystal grains: such rotation can modify the spacing of moiré fringes [33]. To evaluate this effect, we acquired electron diffraction patterns from two points in a $Nd_2Fe_{14}B$ grain, one point near the boundary of the neighboring m-Nd grain, and the other point at a distance of 250 nm from the boundary (not shown here). The observed lattice rotation was 0.2 (±0.2) degrees. Following the equation for rotating moiré patterns [33], this small rotation could modify the fringe spacing by ±0.1%. The precision in the strain measurements will be discussed elsewhere in greater detail. Despite these ambiguities, the observations can indicate the regions in which the $Nd_2Fe_{14}B$ lattice is subjected to significant strain as demonstrated in the subsequent section.

3. Results and discussion

3.1. Strain measurements using artificial moiré fringes

A process to determine the lattice strain ε_c using artificial moiré fringes is explained. In the following analysis, ε_c represents elongation/contraction for the interplanar distance of the *c* plane in the $Nd_2Fe_{14}B$ phase. A map of ε_c is acquired from the $Nd_2Fe_{14}B$ grain indicated by the dot in Fig. 2(a), which is located near a triple junction. Elemental mapping using electron energy-loss spectroscopy, shown in Fig. 2(c)–(f), identifies the triple junction to contain both the m-Nd phase (upper portion) and a Cu-rich region (lower portion; NdCu [13]). The other crystal grains in Fig. 2(a), neighboring the triple junction area, were identified as $Nd_2Fe_{14}B$ and $NdFe_4B_4$. The dark portions in Fig. 2(a) represent cracks.